How to cite: *Angew. Chem. Int. Ed.* **2021**, *60*, 19201 – 19206
International Edition: doi.org/10.1002/anie.202103943
German Edition: doi.org/10.1002/ange.202103943

**Antibacterial Agents**

# Synergistic Lysozyme-Photodynamic Therapy Against Resistant Bacteria based on an Intelligent Upconversion Nanoplatform

*Zhuo Li, Shan Lu,* Wenzhen Liu, Tao Dai, Jianxi Ke, Xingjun Li, Renfu Li, Yuxiang Zhang, Zhuo Chen, and Xueyuan Chen**

***Abstract:*** *The rapid emergence of drug-resistant bacteria has raised a great social concern together with the impetus for exploring advanced antibacterial ways. NIR-triggered antimicrobial photodynamic therapy (PDT) by lanthanide-doped upconversion nanoparticles (UCNP) as energy donor exhibits the advantages of high tissue penetration, broad antibacterial spectrum and less acquired resistance, but is still limited by its low efficacy. Now we designed a bio-inorganic nanohybrid and combined lysozyme (LYZ) with UCNP-PDT system to enhance the efficiency against resistant bacteria. Benefiting from the rapid adhesion to bacteria, intelligently bacteria-responsive LYZ release and synergistic LYZ-PDT effect, the nanoplatform achieves an exceptionally strong bactericidal capacity and conspicuous bacteriostasis on methicillin-resistant S. aureus. These findings pave the way for designing efficiently antibacterial nanomaterials and provide a new strategy for combating deep-tissue bacterial infection.*

## Introduction

Emerging infectious diseases caused by special pathogens pose serious public health problems in worldwide. The current outbreak of COVID-19 epidemic is a devastating example. Equally worrisome is the rising prevalence of resistant bacteria, which could yet be another crisis.[1] The overuse of antibiotics has resulted in a large number of bacteria developing resistance to one or more varieties of antibiotics. These resistant bacteria are much more difficult to treat and associated with high morbidity and mortality.[2] Therefore, it is imperative to develop treatment alternatives that are able to combat resistant-bacteria effectively and avoid new resistance.

Recently, antimicrobial photodynamic therapy (PDT), which utilizes the destructive power of reactive oxygen species (ROS) generated by photosensitizers under light irradiation to inactivate resistant bacteria, has attracted extensive attention.[3] Since PDT does not require specific targeting interaction with bacteria, it gains a competitive advantage in broad antibacterial spectrum and less acquired resistance.[4] At present, PDT has been utilized in clinical treatment of refractory local infectious diseases, such as oral bacterial infections or chronic wounds.[5] What is more, upconversion nanoparticles (UCNP) with the ability of converting near-infrared (NIR) light to visible light, can be served as light sources to activate photosensitizers, allowing for deep-tissue anti-infection treatment.[6]

Yet the antibacterial efficacy of the sole UCNP-PDT system is restricted intrinsically by low upconversion quantum yield and severe hypoxia in infected tissues.[7] Once ROS fail to completely eliminate the bacteria, the residue bacteria will proliferate after PDT treatment. Thus various antibacterial agents such as nitric oxide,[8] silver nanoparticles,[9] copper sulfide,[10] and cationic chitosan[11] have been reported to work in concert to enhance the antibacterial activities. Herein, we pay attention to a more effective and safer antimicrobial agent, lysozyme (LYZ). LYZ is a natural protein that causes bacterial autolysis primarily by hydrolyzing peptidoglycan of cell wall.[12] ROS kill the bacteria rapidly only under light irradiation, while LYZ can offer a complementary effect for long-term inhibition of bacteria. Besides, the meeting of LYZ and PDT may produce a synergistic effect against invading microbes. ROS are featured with extremely short lifetime and diffusion limit in aqueous system, for instance, singlet oxygen ($^1O_2$) has a lifetime of ca. 3.5 μs and can diffuse less than 0.3 μm.[5] The partial destruction of bacterial cell wall by LYZ will be beneficial for ROS attacking the membrane and cytoplasm. Hitherto, the combination of UCNP-PDT and LYZ for antibacterial purpose has not been proposed. To achieve their compositional integration and further validation of the antibacterial synergy are worth exploring.

In this work, we designed an intelligent bio-inorganic nanohybrid to integrate the enzymatic-photodynamic effect against resistant bacteria. In this nanohybrid, hierarchical coating of dense silica and dendritic mesoporous silica on UCNP provided effective loading of methylene blue (MB) as photosensitizer and macromolecular LYZ, respectively. A bacterial hyaluronidase (HAase)-responsive valve was fur-

[*] Z. Li, Dr. S. Lu, Dr. W. Z. Liu, T. Dai, J. X. Ke, Dr. X. J. Li, R. F. Li, Y. X. Zhang, Prof. Z. Chen, Prof. X. Y. Chen
CAS Key Laboratory of Design and Assembly of Functional Nanostructures, State Key Laboratory of Structural Chemistry, and Fujian Key Laboratory of Nanomaterials, Fujian Institute of Research on the Structure of Matter, Chinese Academy of Sciences
Fuzhou, Fujian 350002 (China)
E-mail: lushan@fjirsm.ac.cn
xchen@fjirsm.ac.cn
Z. Li, Dr. S. Lu, Prof. X. Y. Chen
College of Chemistry, Fuzhou University
Fuzhou, Fujian 350116 (China)
Dr. S. Lu, Dr. X. J. Li, Prof. Z. Chen, Prof. X. Y. Chen
Fujian Science and Technology Innovation Laboratory for Optoelectronic Information of China
Fuzhou, Fujian 350108 (China)
Supporting information and the ORCID identification number(s) for the author(s) of this article can be found under: https://doi.org/10.1002/anie.202103943.

  

ther mounted on the particle surface based on layer-by-layer (LBL) assembly of hyaluronic acid (HA) and poly-L-lysine (PLL) to realize intelligent release of LYZ. The resulting nanohybrid could effectively eliminate methicillin-resistant *Staphylococcus aureus* (MRSA) and was successfully applied for the treatment of deep-tissue MRSA infections in vivo.

## Results and Discussion

The antibacterial nanohybrid (designated as UCMB-LYZ-HP) was prepared as schematically illustrated in Figure 1 A. Firstly, β-$NaYF_4$:Yb,Er@$NaYF_4$ core–shell UCNP were synthesized via solid–liquid-thermal decomposition (SLTD) method as described previously.[13] The transmission electron microscopy (TEM, Figure 1 B) image showed that the resulting UCNP were monodisperse and uniform, with a particle size of ca. 100 nm. The XRD pattern (Supporting Information, Figure S1) confirmed the highly crystalline hexagonal phase of the samples. Positively charged MB was in situ encapsulated into silica-coated UCNP by means of reverse microemulsion method (designated as UCMB, Figure 1 C).[14] Subsequently, another layer of dendritic mesoporous silica (DMS) was coated on UCMB by a silica sol-gel reaction with hexadecyltrimethylammonium chloride (CTAC) as the pore template and mesitylene as the pore-expanding agent (Figure 1 D).[15] According to the $N_2$ adsorption-desorption isotherm, the surface area and pore volume of the obtained UCMB@DMS were estimated to be 88 $m^2 g^{-1}$ and 0.2 $cm^3 g^{-1}$, respectively (Figure 1 H). Particularly, UCMB@DMS displayed large mesopores ranging from several to tens of nanometers, which can accommodate a high amount of LYZ. As shown in Figure 1 E, the mesoporous structure of UCMB@DMS became invisible after loading of LYZ. Elemental mappings by scanning transmission electron microscopy (STEM) measurement further revealed the uptake of sulfur-containing LYZ in the nanohybrid (Figure 1 G). HA and PLL were finally assembled on the surface of nanoparticles by LBL method to form an intelligent valve (designated as HP) for controlling the LYZ release (Figure 1 F).[16] The zeta potential measurements showed a clear change for UCMB@DMS from −13.3 mV to +15.3 mV and +30.9 mV after loading of LYZ and HP valve, respectively (Figure 1 I). The products obtained in each synthetic step showed excellent uniformity and monodispersity from TEM images (Figure 1 C–F). Correspondingly, the average hydrodynamic sizes of UCMB, UCMB@DMS, UCMB-LYZ, and UCMB-LYZ-HP were determined to be 135, 219, 230 and 239 nm, respectively, with small polydispersity index (PDI) values (0.034–0.109) (Figure S2).

MB exists in dimer and monomer forms with absorption maxima at 590 and 654 nm, respectively.[17] To achieve a high-yield of $^1O_2$ production, MB was meticulously encapsulated to maintain the monomer form as much as possible (Figure 2 A). Moreover, UCNP with large size of 100 nm and thin inert shell of ca. 3.5 nm for surface passivation exhibited much stronger upconversion luminescence (UCL) as compared with the core-only or small-sized UCNP (27 nm), providing enough energy transferred to MB (Figure 2 B and Figure S3–S7). We then evaluated the ability of UCMB to generate $^1O_2$

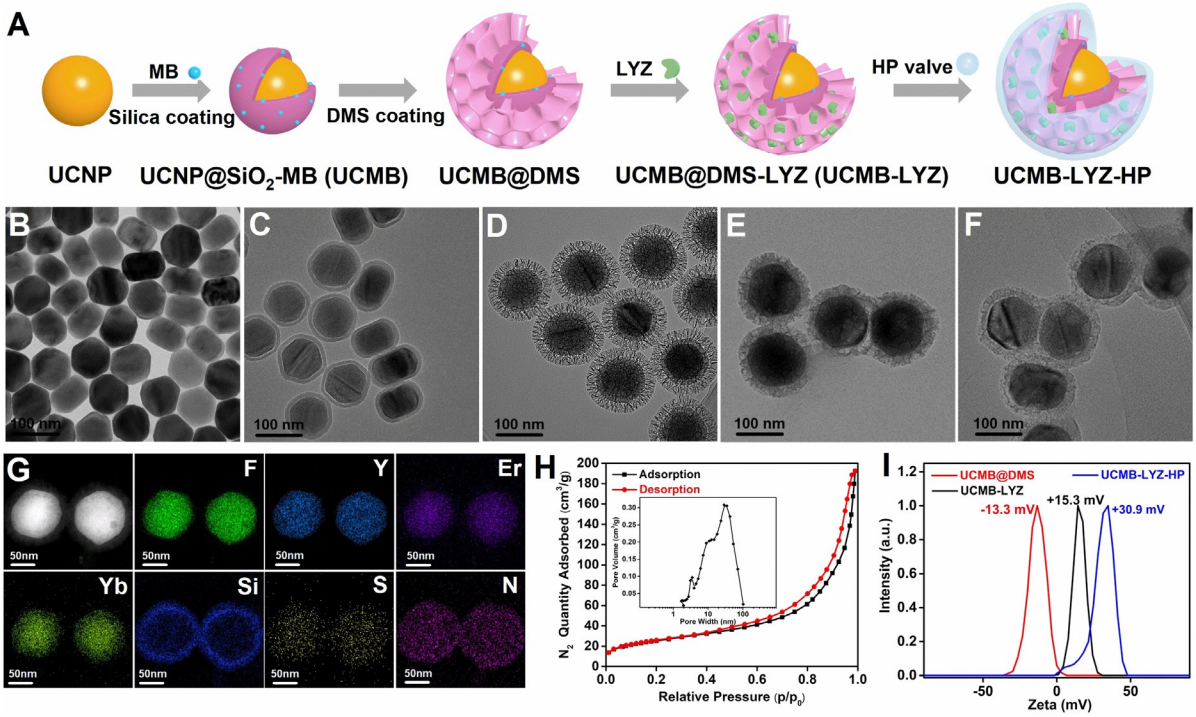


***Figure 1.*** A) Illustration of the fabrication of antibacterial nanohybrid UCMB-LYZ-HP. B)–F) TEM images of (B) β-$NaYF_4$:Yb,Er@$NaYF_4$ (UCNP), (C) UCNP@$SiO_2$-MB (UCMB), (D) UCMB@DMS, (E) UCMB@DMS-LYZ (UCMB-LYZ), and (F) UCMB-LYZ-HP. G) STEM and corresponding elemental (F, Y, Yb, Er, Si, S, N) mappings of UCMB-LYZ-HP. H) $N_2$ adsorption–desorption isotherm and pore size distribution of UCMB@DMS. I) Zeta potentials of UCMB@DMS, UCMB-LYZ, and UCMB-LYZ-HP.

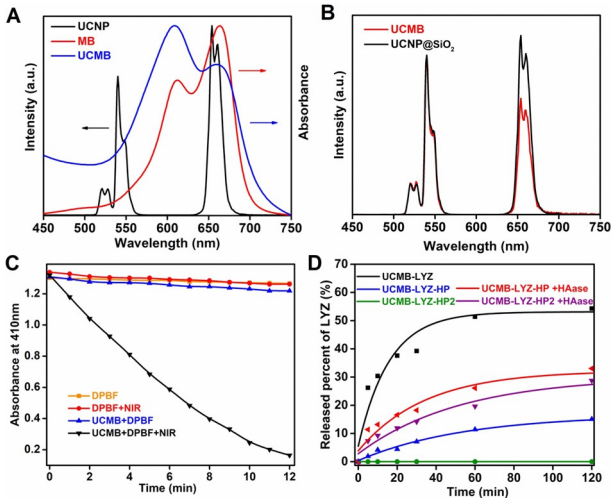


***Figure 2.*** A) UCL spectrum of UCNP and absorption spectra of MB and UCMB. B) UCL spectra of UCNP@$SiO_2$ and UCMB. C) Time-dependent bleaching of DPBF caused by $^1O_2$ generation in the presence of UCMB (1.5 mg mL$^{-1}$) upon NIR laser irradiation at 980 nm (0.5 W cm$^{-2}$). D) Release profiles of LYZ from UCMB-LYZ-HP or UCMB-LYZ nanoparticles under different conditions.

by measuring the bleaching of 1,3-diphenylisobenzonfuran (DPBF) at 410 nm. Without NIR irradiation or UCMB, the absorbance of DPBF remained essentially unchanged. In contrast, the absorbance decreased rapidly to 12% within 12 min at the presence of UCMB under 980-nm irradiation (Figure 2C). The bleaching rate was much more rapid than that of nanohybrid with 27-nm UCNP under identical conditions, where the intensity decreased to 33% (Figure S8).

A high uptake of LYZ (up to 25%, w/w) in the nanohybrid was reached under pH 10 condition due to the charge attraction between LYZ (pI 11) and siliceous surface (p$K_a$ 3.6) (Figure S9). In a neutral biological context, undesired leaching driven by strong protein-protein repulsion may occur immediately.[18] As shown in Figure 2D and Figure S10, most of LYZ was released rapidly from UCMB@DMS in the initial 20 min. The release rate was slowed down after coating of an HP layer and even totally suppressed though a repeated HP coating (for UCMB-LYZ-HP2, Figure S11). With the addition of HAase, an enzyme that can be secreted by bacteria and capable of breaking down HA, LYZ was released gradually from UCMB-LYZ-HP or UCMB-LYZ-HP2. These observations indicated that the release of LYZ in such nanohybrid was well controlled by HP valve and intelligently triggered by bacteria.

MRSA, a common antibiotic-resistant pathogen associated with serious infections was used to evaluate the antibacterial activity of the nanohybrid.[19] We firstly explored and optimized the effect of PDT alone against MRSA by using a non-LYZ counterpart UCMB-HP. All PDT experiments in this work were performed under 980-nm irradiation with a relatively low power density of 0.5 W cm$^{-2}$. The results from spread plate method showed that single PDT treatment caused a reduction of MRSA ranging from 0.5–3 $\log_{10}$ CFU mL$^{-1}$ in comparison to control (Figure 3A,B). The optimized irradiation time and agent concentration were 10 min and 60 μg mL$^{-1}$, respectively. Further increasing irradiation time or concentration resulted in slight enhancement of inactivation rate and might induce overheat effect or toxicity. When MRSA were incubated with UCMB-LYZ-HP for 30-min enzymatic pretreatment and then submitted to PDT, the survival rates of MRSA remarkably decreased at all agent concentrations (Figure 3D). Particularly, 5.2 $\log_{10}$ reduction of MRSA viability was achieved upon the pretreatment of UCMB-LYZ-HP (60 μg mL$^{-1}$) for 30 min and further 10-min NIR illumination. According to infection control guidelines, such an inactivation rate can be defined as a disinfecting effect.[5] The antibacterial activity of UCMB-LYZ-HP without illumination (LYZ treatment alone) was also assessed as parallel, and there was only 1.6 $\log_{10}$ reduction in viable counts of MRSA. Therefore, it could be inferred that the high antibacterial efficacy of the nanohybrid originated from both LYZ and photodynamic inactivation (Figure 3C,E).

In view of the strong bactericidal effect of the nanohybrid in vitro, we further explored its efficacy on deep-tissue MRSA infection. The cytocompatibility of the nanohybrid was evaluated by MTT, showing that the nanohybrid had no cytotoxic effect on human embryonic liver cell line (LO2) (Figure S12). The animal model of deep-tissue localized infection was established by inoculating MRSA into an excisional wound and covering the wound with a piece of pork tissue (5 mm-thick) during PDT treatment. 20 μL of nanohybrid (600 μg mL$^{-1}$) was added to the wounds for incubation (30 min) and then one-time PDT (980 nm irradiation, 10 min) was carried out. Our previous work has excluded the antibacterial effect of only NIR light irradiation and confirmed a higher deep-tissue PDT efficacy under NIR light irradiation than red-light irradiation.[6e] Herein, we performed a comprehensive experiment to demonstrate the combined and individual effect of LYZ and PDT against MRSA, by dividing the mice into four groups including: (i) 20 μL 0.9% saline solution as control; (ii) UCMB-HP + NIR (PDT treatment), (iii) UCMB-LYZ-HP (LYZ treatment), and (iv) UCMB-LYZ-HP + NIR (LYZ + PDT treatment). The typical photographs of MRSA-infected wounds in mice with different treatments were shown in Figure 3F. Compared with the control group, groups receiving LYZ and/or PDT treatment showed obvious healing promotion, and the combined treatment exhibited the best effect. A wound healing rate of 37% was achieved for LYZ + PDT treatment on Day 2, while the values were only about 25% for single treatment and 18% for the control (Figure 3G). After 20 days, the wound area in LYZ + PDT treatment group was calculated as 0.05 cm$^2$ with a wound healing rate over 95% (Figure 3G,H). There was significant difference ($p < 0.01$) in wound area between the groups of combined and individual treatment. Meanwhile, histological analysis of MRSA infected wound tissue was performed. Tissue edema and inflammatory cell infiltration were observed in the wound tissues of both control and nanohybrid treated mice on Day 1. After 20 days, tissues in mice treated with nanohybrid showed only a small amount of inflammatory cell infiltration while control group exhibited a continued presence of inflammation (Figure S13). The local administrated nanohybrid with a very

  

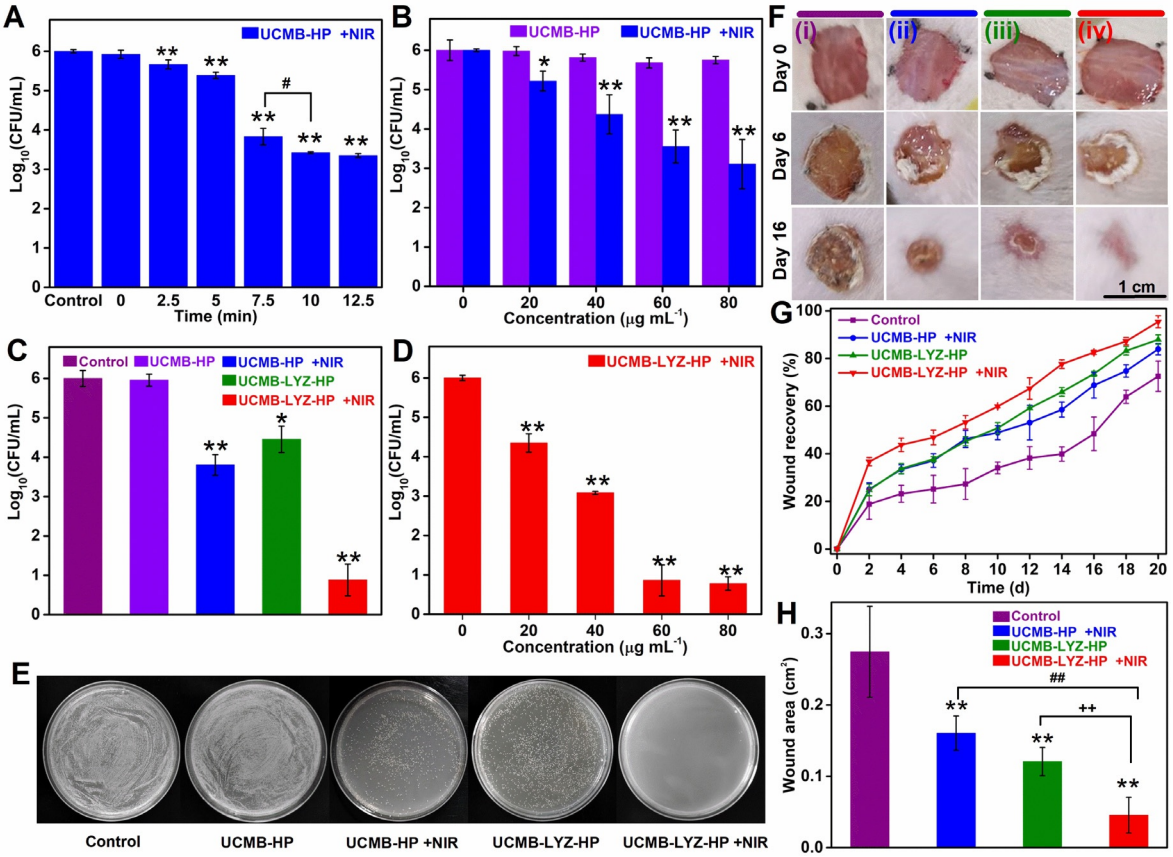


***Figure 3.*** A)–E) In vitro antibacterial effect on MRSA with treatment of different agents: A) survival rates of MRSA treated by UCMB-HP under NIR irradiation (0.5 $Wcm^{-2}$, 0, 2.5, 5, 7.5, 10, and 12.5 min, respectively); B) survival rates of MRSA treated by UCMB-HP at different concentrations under NIR irradiation (0.5 $Wcm^{-2}$, 10 min); C) survival rates of MRSA in different treatment groups; D) survival rates of MRSA treated by UCMB-LYZ-HP at different concentrations under NIR irradiation (0.5 $Wcm^{-2}$, 10 min); and E) photos of the colonies on the LB agar plates of MRSA treated with different agents. F)–H) Therapeutic effect on deep-tissue MRSA infection in different treatment groups ((i) control, (ii) UCMB-HP + NIR, (iii) UCMB-LYZ-HP, and (iv) UCMB-LYZ-HP + NIR, six mice per group): F) typical photographs of MRSA-infected wounds on Days 0, 6 and 16; G) time-dependent wound recovery; and H) comparison of wound areas on Day 20. * and ** indicate significant differences ($P<0.05$ and $P<0.01$, respectively) from the corresponding control group. # and ## indicate significant differences ($P<0.05$ and $P<0.01$, respectively) between the two groups. + and + + indicate significant differences ($P<0.05$ and $P<0.01$, respectively) between the two groups. All experiments involving animals were approved by the Animal Ethics Committee of Fujian Medical University.

low dose (0.4 $mg\,kg^{-1}$) tended to retain in the wound site within the period of experiment and few systemic side effects could be induced.[11b] The weight of mice in each group increased gradually within 20 days, and the organ examination via hematoxylin and eosin (H&E) staining revealed no evident histopathological abnormalities or lesions (Figure S14 and S15). All these findings showcased that the designed nanohybrid with combined efficacy from both LYZ and PDT holds great promise as a safe and effective strategy to combat deep-tissue infection.

For such a highly effective antibacterial nanohybrid, an enzymatic-photodynamic synergistic mechanism was proposed and illustrated in Figure 4A. Firstly, the nanohybrid rapidly adheres to the negatively charged bacteria owing to its highly positive charge (+ 30.9 mV). The binding kinetics of UCMB-LYZ-HP to the bacteria were measured by tracking the fluorescence change of MRSA on a flow cytometer and the binding process was observed to basically complete within 240 s (Figure 4B).[20] The UCL images further confirmed the attachment of nanohybrid with bacteria (Figure 4C). Subsequently, HP layer on nanohybrid was degraded by bacterial HAase, resulting in the release of LYZ.[21] From TEM images in Figure 4D, intact and destroyed cell walls could be clearly observed for the bacteria tethered with UCMB-HP and UCMB-LYZ-HP, respectively. The partial destruction of bacterial cell wall by LYZ facilitated the ROS attacking of bacterial membrane and cytoplasm and accelerated the death of bacteria. The morphology evolution of MRSA during the treatment was revealed by scanning electron microscope (SEM, Figure 4E). The untreated MRSA cells had a spherical shape and a smooth surface. With initial hydrolysis by LYZ, bacterial surfaces were partially wrinkled with circular openings. Upon further NIR exposure, most of the cells were ruptured and multiple lesions and holes were clearly observed in MRSA cells. Meanwhile, the live/dead bacterial staining assay and integrity testing of cell membrane were performed, verifying the gradual destruction of cell membrane and complete bacteria death as the result of synergistic enzymatic hydrolysis and oxidative lesion (Figure 4E and Figure S16). Besides MRSA, the antibacterial effect of nanohybrid on

  

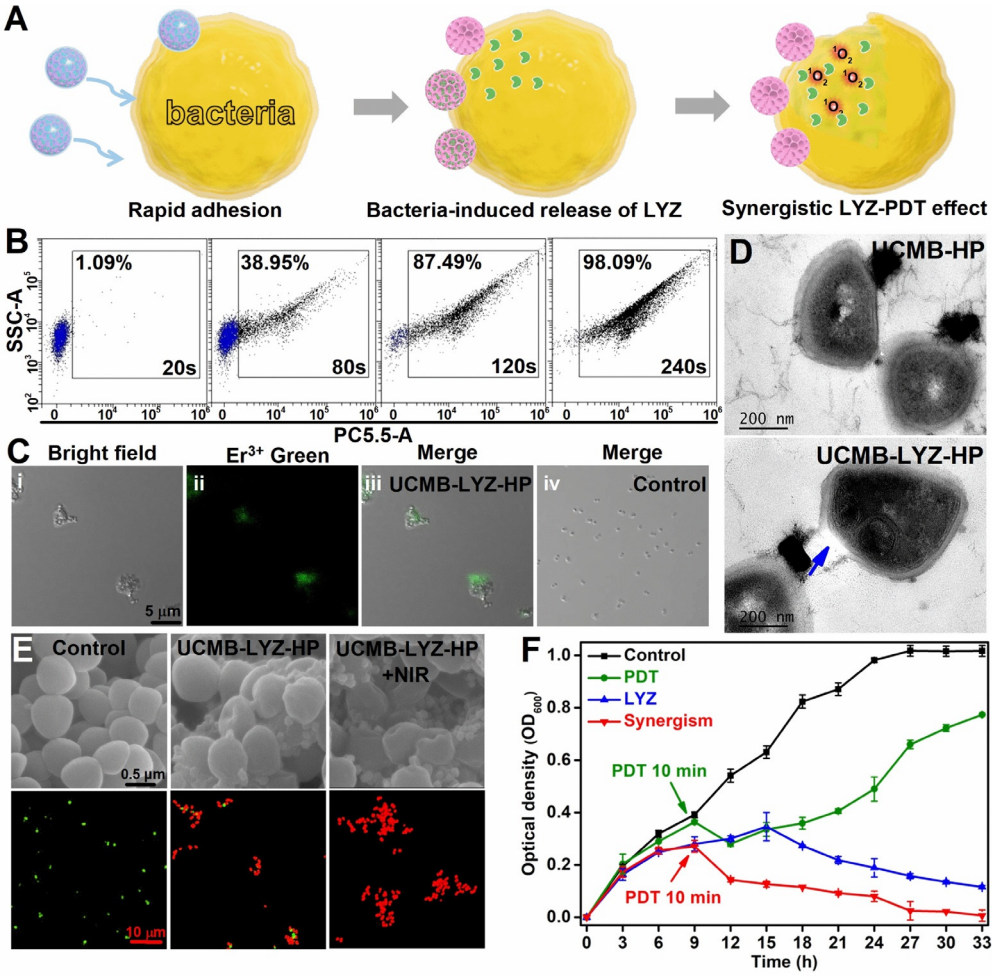


***Figure 4.*** A) Proposed antibacterial mechanism of the nanohybrid based on synergistic enzymatic-photodynamic effect. B) Binding kinetics of UCMB-LYZ-HP to MRSA measured by a flow cytometer. The fluorescent signals of UCMB-LYZ-HP on MRSA increased rapidly within 240 s. (MRSA: $10^7$ CFU mL$^{-1}$, UCMB-LYZ-HP: 60 μg mL$^{-1}$) C) CLSM images of MRSA after incubation with UCMB-LYZ-HP. Panels i and ii show the bright-field image and green UCL image, respectively. Panels iii and iv show the overlay images. D) Representative TEM images of MRSA after incubation with UCMB-HP and UCMB-LYZ-HP, respectively. E) SEM images and overlapping fluorescence images for live/dead staining assay of MRSA bacteria with UCMB-LYZ-HP treatment and further NIR exposure. Dead cells are identified by red-fluorescent PI staining. The green or red fluorescence is defined as live or dead cells, respectively. F) Growth curves of MRSA for different treatments. The optical density of all treatments at time zero have been subtracted from subsequent measurements.

another bacteria, multidrug-resistant *Escherichia coli* (MDR *E. coli*), was also assessed. The results showed that enzymatic treatment can also enhance the photodynamic inactivation with reduction of MDR *E. coli* viability from 4.5 $\log_{10}$ to 3.5 $\log_{10}$ (Figure S17). Compared with Gram-positive bacteria MRSA, the synergistic antibacterial effect on Gram-negative bacteria MDR *E. coli* was not so significant. These findings can be well explained by the main cell wall-lytic mechanism of LYZ and further support our proposed synergistic antibacterial mechanism for the nanohybrid.

To highlight the synergistic antibacterial effect, a long-term real-time bacterial inhibition ability of the nanohybrid was further evaluated. As shown in Figure 4F, MRSA without any treatment proliferated in the culture medium with an increased optical density at 600 nm ($OD_{600}$). MRSA incubated with UCMB-HP exhibited a similar growth curve at initial state. A reduction of 0.1 $OD_{600}$ was noted immediately post PDT treatment at 9 h but the value increased again in the following 24 h. $OD_{600}$ of MRSA suspensions incubated with UCMB-LYZ-HP showed a slower increase and began to decrease after 15 h. With additional PDT treatment at 9 h, MRSA growth sharply decreased and then continued down to complete inhibition in 33 h. These observations suggest that LYZ enables PDT more efficacious against MRSA and conspicuous bacteriostasis can only be accomplished by utilizing the synergistic effect of LYZ and PDT.

## Conclusion

A well-defined nanohybrid UCMB-LYZ-HP has been successfully synthesized with the designed features of HAase-mediated release of LYZ and superior production of $^1O_2$. In vitro experiments showed that the nanohybrid had a strong disinfecting effect against pathogenic bacteria (>5 $\log_{10}$ reduction of MRSA viability). More significantly, we achieved excellent therapeutic efficacy against deep-tissue (5 mm-thick) MRSA infections without causing any side effects in murine model. We further examined the mechanism of nanohybrid, demonstrating a high affinity towards bacteria, rapid response and the synergistic effect via LYZ disrupting of the cell wall and exposing the bacteria to ROS. This synergistic LYZ-PDT strategy is superior to the simple PDT treatment, which not only improves the bactericidal efficiency, but also prolongs the antibacterial activity, so as to eliminate infection and avoid recurrence. Our work may open up a new avenue for the exploration of efficiently synergistic anti-resistant bacterial agents.

## Acknowledgements

This work was supported by the Science and Technology Cooperation Fund between Chinese and Australian Governments (no. 2017YFE0132300), the Strategic Priority Research Program of the CAS (no. XDB20000000), the NSFC (nos. 51672272, 21771185, 21771178, 21975257, 81572944, 81971983), Youth Innovation Promotion Association of CAS (no. 2017347), and the CAS/SAFEA International Partnership Program for Creative Research Teams.

## Conflict of Interest

The authors declare no conflict of interest.

**Keywords:** antibacterial agents · enzymes · mesoporous materials · photodynamic therapy · upconversion nanoparticles

[1] a) W. Gao, L. Zhang, *Nat. Rev. Microbiol.* **2021**, *19*, 5 – 6; b) E. Martens, A. L. Demain, *J. Antibiot.* **2017**, *70*, 520 – 526; c) J. N. Spijk, S. Schmitt, A. Schoster, *Equine Vet. Educ.* **2019**, *31*, 653 – 658.

[2] a) R. I. Aminov, *Front. Microbiol.* **2010**, *1*, 134; b) H. F. Chambers, F. R. Deleo, *Nat. Rev. Microbiol.* **2009**, *7*, 629 – 641; c) M. Garvey, *Antibiotics* **2020**, *9*, 414; d) K. S. Kaye, J. M. Pogue, *Pharmacotherapy* **2015**, *35*, 949 – 962.

[3] a) M. R. Hamblin, T. Hasan, *Photochem. Photobiol. Sci.* **2004**, *3*, 436 – 450; b) T. Maisch, *Lasers Med. Sci.* **2007**, *22*, 83 – 91; c) R. Yin, T. Agrawal, U. Khan, G. K. Gupta, V. Rai, Y. Huang, M. R. Hamblin, *Nanomedicine* **2015**, *10*, 2379 – 2404; d) Z. Zhao, R. Yan, J. Wang, H. Wu, Y. Wang, A. Chen, S. Shao, Y. Q. Li, *J. Mater. Chem. B* **2017**, *5*, 3572 – 3579; e) S. Pierce, M. P. Jennings, S. A. Juliano, A. M. Angeles-Boza, *Inorg. Chem.* **2020**, *59*, 14866 – 14870.

[4] a) Q. Jia, Q. Song, P. Li, W. Huang, *Adv. Healthcare Mater.* **2019**, *8*, 1900608; b) J. Krajczewski, K. Rucińska, H. E. Townley, A. Kudelski, *Photodiagn. Photodyn. Ther.* **2019**, *26*, 162 – 178; c) H. Mahmoudi, A. Bahador, M. Pourhajibagher, M. Y. Alikhani, *J. Lasers. Med. Sci.* **2018**, *9*, 154 – 160; d) K. Zhou, R. Tian, G. Li, X. Qiu, L. Xu, M. Guo, D. Chigan, Y. Zhang, X. Chen, G. He, *Chem. Eur. J.* **2019**, *25*, 13472 – 13478.

[5] F. Cieplik, D. Deng, W. Crielaard, W. Buchalla, E. Hellwig, A. Al-Ahmad, T. Maisch, *Crit. Rev. Microbiol.* **2018**, *44*, 571 – 589.

[6] a) J. Li, Q. Zhao, F. Shi, C. Liu, Y. Tang, *Adv. Healthcare Mater.* **2016**, *5*, 2967 – 2971; b) J. Liu, M. Yu, G. Zeng, J. Cao, Y. Wang, T. Ding, X. Yang, K. Sun, J. Parvizi, S. Tian, *J. Mater. Chem. B* **2018**, *6*, 7854 – 7861; c) Z. Nie, X. Ke, D. Li, Y. Zhao, L. Zhu, R. Qiao, X. L. Zhang, *J. Phys. Chem. C* **2019**, *123*, 22959 – 22970; d) Y. Ye, Y. Li, F. Fang, *Int. J. Nanomed.* **2014**, *9*, 5157 – 5165; e) Y. Zhang, P. Huang, D. Wang, J. Chen, W. Liu, P. Hu, M. Huang, X. Chen, Z. Chen, *Nanoscale* **2018**, *10*, 15485 – 15495; f) W. You, D. Tu, W. Zheng, P. Huang, X. Chen, *J. Lumin.* **2018**, *201*, 255 – 264; g) W. Liu, Y. Zhang, W. You, J. Su, S. Yu, T. Dai, Y. Huang, X. Chen, X. Song, Z. Chen, *Nanoscale* **2020**, *12*, 13948 – 13957; h) Y. Yang, J. Aw, B. Xing, *Nanoscale* **2017**, *9*, 3698 – 3718.

[7] a) Y. Huang, F. Qiu, R. Chen, D. Yan, X. Zhu, *J. Mater. Chem. B* **2020**, *8*, 3772 – 3788; b) H. Möllerherm, K. Branitzki-Heinemann, G. Brogden, A. A. Elamin, W. Oehlmann, H. Fuhrmann, M. Singh, H. Y. Naim, M. von Köckritz-Blickwede, *Front. Immunol.* **2017**, *8*, 541; c) C. Duan, L. Liang, L. Li, R. Zhang, Z. P. Xu, *J. Mater. Chem. B* **2018**, *6*, 192 – 209.

[8] J. Sun, Y. Fan, L. Tian, S. Niu, W. Ming, J. Zhao, L. Ren, *Chem. Eng. J.* **2020**, 1385 – 8947.

[9] Y. Zhao, M. Hu, Y. Zhang, J. Liu, C. Liu, S. K. Choi, Z. Zhang, L. Song, *Chem. Eng. J.* **2020**, *385*, 123980.

[10] M. Yin, Z. Li, E. Ju, Z. Wang, K. Dong, J. Ren, X. Qu, *Chem. Commun.* **2014**, *50*, 10488 – 10490.

[11] a) X. Ding, S. Duan, X. Ding, R. Liu, F.-J. Xu, *Adv. Funct. Mater.* **2018**, *28*, 1802140; b) S. Li, S. Cui, D. Yin, Q. Zhu, Y. Ma, Z. Qian, Y. Gu, *Nanoscale* **2017**, *9*, 3912 – 3924.

[12] a) D. M. Chipman, N. Sharon, *Science* **1969**, *165*, 454 – 465; b) A. J. Kirby, *Nat. Struct. Biol.* **2001**, *8*, 737 – 739.

[13] W. You, D. Tu, W. Zheng, X. Shang, X. Song, S. Zhou, Y. Liu, R. Li, X. Chen, *Nanoscale* **2018**, *10*, 11477 – 11484.

[14] a) H. Wang, R. L. Han, L. M. Yang, J. H. Shi, Z. J. Liu, Y. Hu, Y. Wang, S. J. Liu, Y. Gan, *ACS Appl. Mater. Interfaces* **2016**, *8*, 4416 – 4423; b) S. Lu, D. Tu, P. Hu, J. Xu, R. Li, M. Wang, Z. Chen, M. Huang, X. Chen, *Angew. Chem. Int. Ed.* **2015**, *54*, 7915 – 7919; *Angew. Chem.* **2015**, *127*, 8026 – 8030.

[15] a) B. Ding, S. Shao, C. Yu, B. Teng, M. Wang, Z. Cheng, K. L. Wong, P. Ma, J. Lin, *Adv. Mater.* **2018**, *30*, 1802479; b) J. Tang, A. K. Meka, S. Theivendran, Y. Wang, Y. Yang, H. Song, J. Fu, W. Ban, Z. Gu, C. Lei, S. Li, C. Yu, *Angew. Chem. Int. Ed.* **2020**, *59*, 22054 – 22062; *Angew. Chem.* **2020**, *132*, 22238 – 22246; c) Y. Dai, D. Yang, D. Yu, S. Xie, B. Wang, J. Bu, B. Shen, W. Feng, F. Li, *Nanoscale* **2020**, *12*, 5075 – 5083.

[16] a) A. Ivanova, K. Ivanova, J. Hoyo, T. Heinze, S. Sanchez-Gomez, T. Tzanov, *ACS Appl. Mater. Interfaces* **2018**, *10*, 3314 – 3323; b) Y. Wu, Y. Long, Q. L. Li, S. Han, J. Ma, Y. W. Yang, H. Gao, *ACS Appl. Mater. Interfaces* **2015**, *7*, 17255 – 17263.

[17] F. Chen, S. Zhang, W. Bu, Y. Chen, Q. Xiao, J. Liu, H. Xing, L. Zhou, W. Peng, J. Shi, *Chem. Eur. J.* **2012**, *18*, 7082 – 7090.

[18] a) L. L. Li, H. Wang, *Adv. Healthcare Mater.* **2013**, *2*, 1351 – 1360; b) S. Lu, Z. An, J. Li, J. He, *J. Phys. Chem. B* **2011**, *115*, 13695 – 13700; c) S. Lu, J. He, Z. Liu, *Chem. Eng. J.* **2009**, *146*, 503 – 514.

[19] A. S. Lee, H. de Lencastre, J. Garau, J. Kluytmans, S. Malhotra-Kumar, A. Peschel, S. Harbarth, *Nat. Rev. Dis. Primers* **2018**, *4*, 18033.

[20] a) Y. Zhang, K. Zheng, Z. Chen, J. Chen, P. Hu, L. Cai, Z. Iqbal, M. Huang, *Appl. Microbiol. Biotechnol.* **2017**, *101*, 4691 – 4700; b) J. Sun, Y. Zhang, J. Su, T. Dai, J. Chen, L. Zhang, H. Wang, W. Liu, M. Huang, Z. Chen, *Dyes Pigm.* **2020**, *179*, 108392.

[21] W. L. Hynes, S. L. Walton, *FEMS Microbiol. Lett.* **2000**, *183*, 201 – 207.

Manuscript received: March 19, 2021
Revised manuscript received: May 14, 2021
Accepted manuscript online: June 16, 2021

  